Quantum-Chemical Calculations on the Mechanism of the Water–Gas Shift Reaction on Nanosized Gold Cluster

ARTICLE *in* THE JOURNAL OF PHYSICAL CHEMISTRY C · JANUARY 2012

Impact Factor: 4.77 · DOI: 10.1021/jp209172w

5 AUTHORS, INCLUDING:

Hui-Lung Chen
Chinese Culture University
64 PUBLICATIONS **441** CITATIONS
SEE PROFILE

Shin-Pon Ju
National Sun Yat-sen University
136 PUBLICATIONS **920** CITATIONS
SEE PROFILE

Hsin-Tsung Chen
Chung Yuan Christian University
78 PUBLICATIONS **703** CITATIONS
SEE PROFILE

THE JOURNAL OF PHYSICAL CHEMISTRY C

ARTICLE

pubs.acs.org/JPCC

Quantum-Chemical Calculations on the Mechanism of the Water−Gas Shift Reaction on Nanosized Gold Cluster

Ren-Jie Lin,[†] Hui-Lung Chen,[‡] Shin-Pon Ju,[§] Feng-Yi Li,[*,†] and Hsin-Tsung Chen[*,⊥]

[†]Department of Chemistry, National Chung Hsing University, Taichung 402, Taiwan

[‡]Department of Chemistry and Institute of Applied Chemistry, Chinese Culture University, Taipei, 111,Taiwan

[§]Department of Mechanical and Electro-Mechanical Engineering; Center for Nanoscience and Nanotechnology, National Sun Yat-Sen University, Kaohsiung 80424, Taiwan

[⊥]Department of Chemistry, Chung Yuan Christian University, Chungli 32023, Taiwan

ABSTRACT: We have studied the mechanism of the water−gas shift reaction (WGS, $CO + H_2O \rightarrow CO_2 + H_2$) catalyzed by nanosized gold particles by using density functional theory calculations. The molecular structures and adsorbate/substrate interaction energies of H_2O/Au_{38}, CO/Au_{38}, HO/Au_{38}, and H/Au_{38} configurations were predicted. Several adsorption sites on the Au_{38} nanoparticle were considered in this study and characterized as top, bridge, hollow, and hcp sites. A potential energy surface for WGS reaction on the Au_{38} nanoparticle has been constructed using the nudged elastic band method. It was found that water dissociation ($H_2O \rightarrow H + OH$) is the rate-limiting step, with an energy barrier of 31.41 kcal/mol. The overall reaction $CO + H_2O + Au_{38} \rightarrow CO_2 + H_2 + Au_{38}$ is exothermic by 16.18 kcal/mol. To gain insights into the high catalytic activity of the gold nanoparticles, the nature of the interaction between adsorbate and substrate is also analyzed by the detailed electronic local density of states.

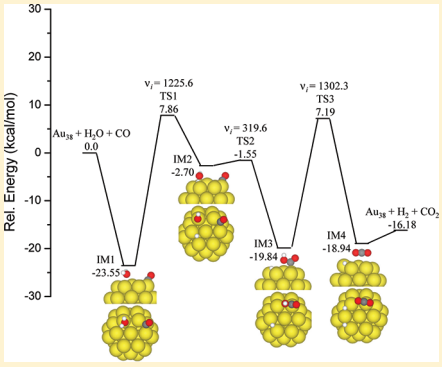

INTRODUCTION

The water−gas shift (WGS) reaction, $CO + H_2O \rightarrow CO_2 + H_2$, is a critical process in providing clean hydrogen for polymer electrolyte membrane fuel cells and other industrial applications.[1−3] Large-scale production of H_2, as envisioned for the hydrogen economy[4−10] (for instance, in connection with hydrogen fuel cells) has sparked renewed interest in finding improved WGS reaction catalysts. Recently there has been a great amount of interest in nanosized gold particles, mostly because of their unusual and unanticipated catalytic properties,[11−15] which are distinctively different from catalytic properties of bulk gold metal. Furthermore, many experimental studies have demonstrated that gold nanoparticles on different oxide supports can act as catalysts at lower temperatures as compared with regular catalysts or even below room temperature.[11,16] It was suggested that these oxides may play a vital role in the catalytic reactions.

The supporting oxides of Au/oxide catalysts can be divided into two types: (i) reducible oxides, such as TiO_2, CeO_2, Fe_2O_3, or IrO_2; and (ii) nonreducible oxides, such as MgO, Al_2O_3, or SiO_2.[17−22] The Au/reducible oxides provide better reactivity for CO oxidation than the nonreducible counterparts due to the defect effect of reducible oxides. However, the remarkable catalytic properties might in part arise from the strong electronic interactions in the Au/oxide catalysts. Recently, Turner et al.[14] reported that very small gold nanoparticles (smaller than 1.4 nm) supported on inert materials, which are chemically inert and do not show electronic interaction with the Au nanoparticles, can act as efficient and robust catalysts for the selective oxidation by O_2. Their results suggest that the higher catalytic activity is due to the altered electronic structure of small gold nanoparticles. Theoretical studies have shown that unsupported Au nanoparticles can be very reactive in the CO oxidation reaction.[23−30] The reason for this enhanced activity is not yet fully understood. The quantum size, electronic effects, thickness, shape, oxidation state, low coordinated sites, and strain of gold nanoparticles have been suggested as the factors for the high catalytic activity of the gold nanoparticles with the oxide support.[23−30] In this work, we applied periodic density functional calculations to investigate the WGS process on the Au_{38} nanoparticle, which had been shown to be the size threshold for epoxidation catalysis,[24] in relation to the adsorption, electronic structure, and activation energy barriers. We believe that this study is vital for understanding the factors governing the WGS oxidation catalyzed by nanosized gold clusters.

COMPUTATIONAL METHOD

The calculations of the WGS reaction were performed using the spin-polarized density functional theory (DFT)[31] with plane wave basis set, as implemented in the Vienna ab initio simulation package (VASP) program.[32−36] The generalized gradient approximation[37] with PW91 functional[38] was adopted along with the projector augmented wave (PAW) potential to describe the interaction between core and valence electrons. The open-shell

Received: September 22, 2011
Revised: December 7, 2011
Published: December 15, 2011

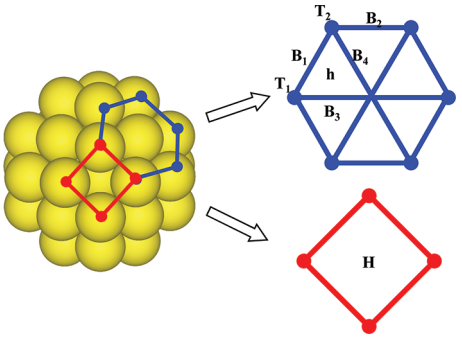

Figure 1. Schematic presentation of Au_{38} nanoparticle. High symmetry adsorption sites on a hexagonal face of the Au_{38} nanoparticle. T_1 and T_2 represent the top sites; B_1, B_2, B_3, and B_4 represent the bridge sites; H represents the hole site ; h represents the hcp site.

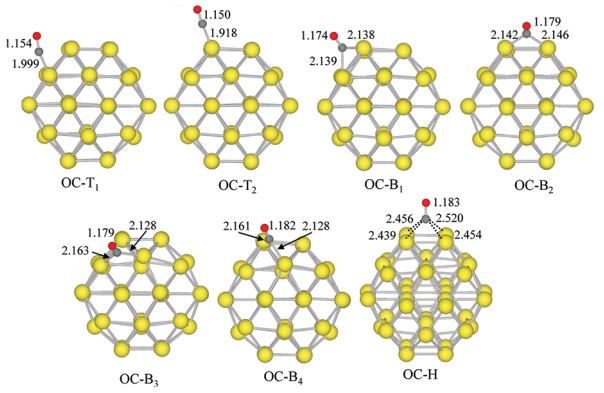

Figure 2. Located isomers of adsorbed CO on the Au_{38} nanoparticle and their important geometric parameters calculated at the PW91 level of theory. The bond lengths are given in angstroms.

spin states of the radical intermediates, such as OH and H radicals, were set as ISPIN = 2 in the calculations. During the DFT calculation, a periodic array composed of Au_{38} each in a cubic supercell was employed with a lattice constant large enough to avoid possible interaction between the cluster and its periodic images.

To find the suitable lattice constant, we used the CO adsorption on Au_{38} with the most stable structure as an example to perform calculations in 20 × 20 × 20, 25 × 25 × 25, and 30 × 30 × 30 $Å^3$ cubic boxes, respectively. It was shown that the cell size effect is negligible when the lattice constant is larger than 25 Å. Therefore the 25 × 25 × 25 $Å^3$ cubic supercell was used for the entire calculation. A 400 eV cutoff energy, which allows convergence to 1×10^{-4} eV in total energy, was used. The Γ point was used for the summation in the Brillouin zone due to the large supercell. In this work, we calculated the adsorption energies according to

$$\Delta E_{ads} = E_{Total} - E_{Au_{38}} - E_{adsorbate} \quad (1)$$

where E_{total}, $E_{Au_{38}}$ and $E_{adsorbate}$ correspond to the electronic energies of adsorbed species on the Au_{38} nanoparticle, the bare Au_{38} nanoparticle, and the gas-phase adsorbate, respectively. Furthermore, the coadsorption energies of CO with H_2O molecule were calculated as

$$\Delta E_{coads} = E_{Total} - E_{Au_{38}} - E_{Co} - E_{H_2O} \quad (2)$$

The nudged elastic band (NEB) method[39,40] was applied to map out minimum-energy paths (MEP) by connecting reactants, intermediates, and product. All transition states were verified by the number of imaginary frequencies (NIMG) with NIMG = 1. Atomic charges of the selected structures were calculated by utilizing the Bader charge analysis[41,42] with a program designed by Henkelman et al.[43]

RESULT AND DISCUSSION

The structure of Au_{38} is modeled as a tetrakaidecahedral structure with the O_h symmetry, which is first optimized to make the Au_{38} configuration coincident with the previous theoretical studies.[25] The calculated average nearest-neighbor bond distance is 2.77 Å, which is in excellent agreement with the experimental value of 2.78 Å,[44] by using the present method. As shown in Figure 1, there are eight equivalent hexagonal fcc(111)-like faces and six equivalent square fcc(100)-like faces in the Au_{38} cluster. Several adsorption sites on the Au_{38} nanoparticle are considered in this study and characterized as top (T), bridge (B), hollow (H), and hcp (h) sites, as shown in Figure 1. For the T site, the species adsorbs on the top of Au atom of Au_{38}. At the B site, the species adsorbs above the center of Au−Au bond between the two nearest Au atoms. At the H sites, the species adsorbs above the center of square of Au_{38}. At the h sites, the species adsorbs above the center of triangle facet of Au_{38}.

Adsorption of CO, H_2O, OH, and H on Au_{38} Nanoparticle. To locate possible stable adsorption configurations of intermediates, such as Au_{38}−CO, Au_{38}−H_2O, Au_{38}−OH, and Au_{38}−H, we placed CO, H_2O, OH, and H species at various sites on the Au_{38} nanoparticle as shown in Figure 1. For CO adsorption, the molecule prefers the "end-on" configurations with a C atom binding to the Au atom. As expected, the CO molecule can adsorb on the Au_{38} nanoparticle in several isomeric structures (see Figure 2) according to the adsorption sites. The related adsorption energies are listed in Table 1. The OC-T_2 and OC-B_1 configurations with adsorption energies as −20.15 and −20.09 kcal/mol, respectively, are energetically the most stable among all the calculated Au_{38}−CO adsorptions. These calculated adsorption energies are close to their counterparts in Au_{32} (−25.4 kcal/mol from the PW91 functional),[29] Au_{29} (−23.3 to approximately −21.0 kcal/mol from the PW91 level),[30] and Au_{10} (−21.9 kcal/mol from the revised Perdew−Burke−Ernzerhof functional)[28] clusters. For Au_{38}−H_2O adsorption, the adsorption energies for all structures as found in this study are within −0.74 to approximately −6.38 kcal/mol, as shown in Table 2. The adsorption of Au_{38}−H_2O is characterized as a physisorbed state as a result of the small adsorption energy. However, the H_2O-T_1 configuration (see Figure 3) is energetically the most stable among all the calculated Au_{38}−H_2O adsorptions.

In addition, we performed a detailed analysis by decomposing the adsorption energy into three individual parts: the relaxation energy of the Au_{38} cluster, the distortion energy of CO (or H_2O) molecule, and the energy of interaction between CO (or H_2O) and the Au_{38} cluster. As described by Delbecq et al.,[45] the relaxation, distortion, and interaction energies were calculated according to the following equations:

$$E_{relaxation} = E[\text{distorted cluster}] - E[\text{cluster}]$$

$$E_{distortion} = E[\text{distorted adsorbate}] - E[\text{adsorbate}]$$

$$E_{interaction} = E_{adsorption} - E_{relaxation} - E_{distortion}$$

dx.doi.org/10.1021/jp209172w |J. Phys. Chem. C 2012, 116, 336–342

Table 1. Calculated Adsorption Energies (in kcal/mol), Geometrical Parameters (Å) of Adsorbed CO Species on Au_{38} Nanoparticle

CO adsorption site	adsorption energy	relaxation energy	distortion energy	interaction energy[a]	d(Au−C)	d(C−O)
OC-T_1	−17.16	1.79	0.18	−19.12	1.999	1.154
OC-T_2	−20.09	1.27	0.07	−21.43	1.971	1.150
OC-B_1	−20.15	3.37	1.22	−24.75	2.139/2.137	1.174
OC-B_2	−18.24	4.03	1.67	−23.94	2.142/2.146	1.179
OC-B_3	−17.93	6.46	1.66	−26.05	2.127/2.163	1.179
OC-B_4	−17.92	5.53	1.89	−25.34	2.128/2.161	1.181
OC-H	−20.09	1.27	0.07	−21.43	1.971	1.150

[a] Interaction energy = adsorption energy − relaxation energy − distortion energy.

Table 2. Calculated Adsorption Energies (in kcal/mol), Geometrical Parameters (Å) of Adsorbed H_2O Species on Au_{38} Cluster

H_2O adsorption site	adsorption energy	relaxation energy	distortion energy	interaction energy	d(Au−O)	d(O−H)
H_2O-T_1	−6.38	0.16	0.02	−6.56	2.559	0.973/0.974
H_2O-T_2	−6.24	0.17	0.07	−6.48	2.495	0.971/0.972
H_2O−B_1	−3.42	0.30	0.07	−3.79	2.869/2.848	0.973/0.974
H_2O−B_2	−6.09	−1.65	0.03	−4.47	2.888/2.916	0.974/0.972
H_2O−H	−1.64	0.46	0.06	−2.15	3.188/3.210	0.973/0.978

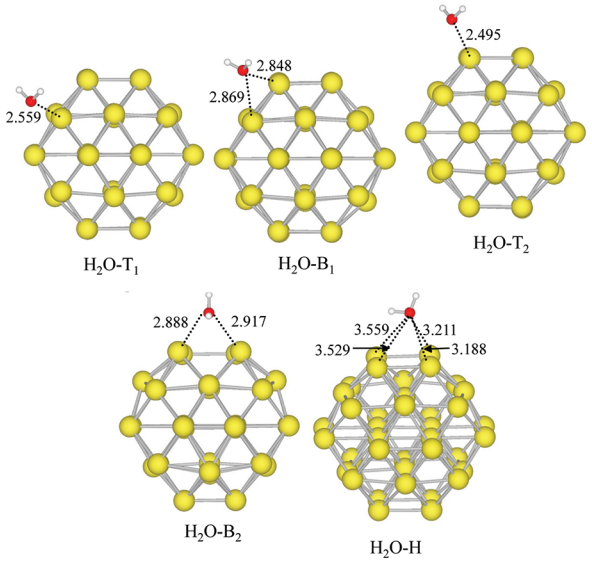

Figure 3. Located isomers of adsorbed H_2O on Au_{38} nanoparticle and their important geometric parameters calculated at the PW91 level of theory. The bond lengths are given in angstroms.

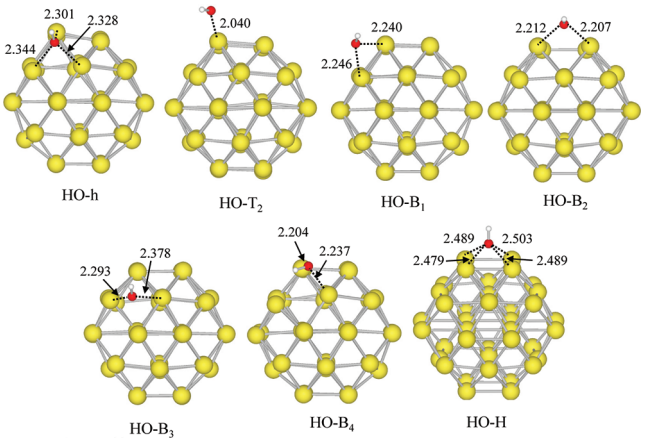

Figure 4. Located isomers of the adsorbed OH on the Au_{38} nanoparticle and their important geometric parameters calculated at the PW91 level of theory. The bond lengths are given in angstroms.

The relaxation and distortion energies ($E_{relaxation}$ and $E_{distortion}$) are the energetic costs for bringing the cluster and the adsorbate from their original separate equilibrium geometry to the geometry they have in the final system, and the interaction energy ($E_{interaction}$) is the energy change that takes place as the two components in their deformed geometries approach each other. The results of these calculations are also included in Tables 1 and 2.

Comparing the computed results for OC-B_1 and OC-T_2, it is found that the relaxation and distortional energies of OC-B_1 are obviously larger than those of the OC-T_2. These surprising results indicate that the Au_{38} cluster in OC-B_1 configuration strongly distorts the CO molecule and destabilizes the substrate structure. Consequently, for the comparison of gas-cluster restructuring between OC-B_1 and OC-T_2, the contribution with the larger interaction energy (ca. −24.75 kcal/mol) of OC-B_1 explains its greater stability of all calculated CO/Au_{38} structures. As shown in Table 2, the top site adsorbed H_2O geometries have two larger adsorption energies (H_2O-T_1 and H_2O-T_2). However, the associated distortional energies of all adsorption sites are quite small (less than ∼0.1 kal/mol), indicating that the water adsorption over all positions of the Au_{38} cluster cannot create effectual distortion to the H_2O moiety.

The interactions, structures, and energies of the Au_{38}−OH and Au_{38}−H are discussed for exploring the WGS reaction on the Au_{38} nanoparticle. As expected, the OH and H radicals adsorb on the Au_{38} nanoparticle, leading to several isomeric structures according to the adsorption sites. The optimized structures of Au_{38}−OH and Au_{38}−H are depicted in Figures 4 and 5.Their adsorption energies are summarized in Tables 3 and 4. It is shown

dx.doi.org/10.1021/jp209172w |J. Phys. Chem. C 2012, 116, 336–342

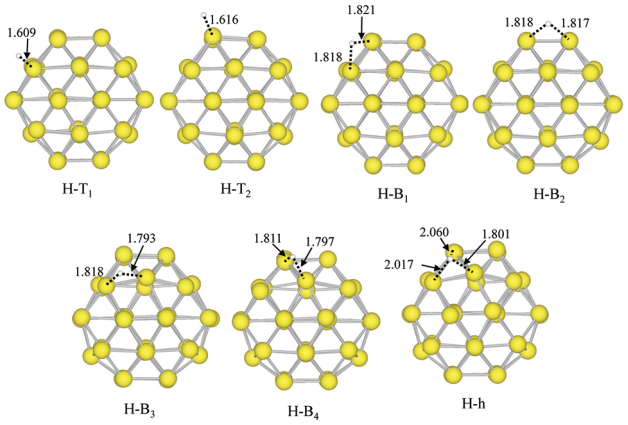

Figure 5. Located isomers of the adsorbed H atom on the Au_{38} nanoparticle and their important geometric parameters calculated at the PW91 level of theory. The bond lengths are given in angstroms.

Table 3. Calculated Adsorption Energies (in kcal/mol), Geometrical Parameters (Å) of Adsorbed OH Species on the Au_{38} Cluster

OH ads. site	adsorption energy	*d*(Au−O)	*d*(O−H)
HO-T_2	−63.51	2.040	0.972
HO-B_1	−66.41	2.246/2.240	0.976
HO-B_2	−72.06	2.212/2.207	0.974
HO-B_3	−61.57	2.293/2.378	0.963
HO-B_4	−61.83	2.204/2.237	0.975
HO-H	−62.82	2.479/2.489/2.503/2.489	0.980
HO-hcp	−65.17	2.344/2.301/2.328	0.977

Table 4. Calculated Adsorption Energies (in kcal/mol), Geometrical Parameters (Å) of the Adsorbed H Atom on the Au_{38} Cluster

H atom adsorption site	adsorption energy (kcal/mol)
H-T_1	−57.24
H-T_2	−57.24
H−B_1	−55.17
H−B_2	−56.29
H−B_3	−56.87
H−B_4	−56.69
H-hcp	−54.53

that the radical adsorbates of OH and H adsorb strongly onto the Au_{38} nanoparticle. The HO-B_2 adsorption is favored with an adsorption energy of 72.06 kcal/mol. The O−H bond length is calculated to be 0.974 Å, which is somewhat longer than that in the gas phase of the HO radical (0.969 Å). The adsorption energies for other structures of Au_{38}−OH are slightly different, within −66.41 to approximately −61.57 kcal/mol, as shown in Table 3. For H adsorption, the adsorption energies for all the structures of Au_{38}−H are slightly different and ranging between −57.24 and −54.54 kcal/mol (see Table 4). The T-H configuration is energetically most stable, with an adsorption energy of −57.2 kcal/mol, and the Au−H bond distance is 1.609 Å.

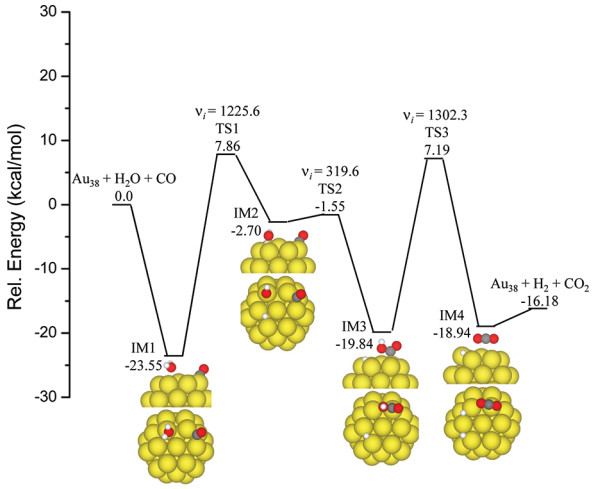

Figure 6. Calculated possible potential energy diagram for the reaction of H_2O and CO on the Au_{38} cluster, where the numbers are the relative energy in kcal/mol and represent the imaginary frequency of a particular transition state. All energies are related to the isolated reactants.

Reaction Profile for WGS Reaction on the Au_{38} Nanoparticle. The generally accepted reaction mechanism[5,6] with the minimum energy barriers for WGS reaction involves the following steps:

$$CO_{(g)} \leftrightarrow CO_{(ads)}$$

$$H_2O_{(g)} \leftrightarrow H_2O_{(ads)}$$

$$H_2O_{(ads)} \rightarrow H_{(ads)} + OH_{(ads)}$$

$$CO_{(ads)} + OH_{(ads)} \rightarrow OCOH_{(ads)}$$

$$OCOH_{(ads)} \rightarrow CO_{2(ads)} + H_{(ads)}$$

$$CO_{2(ads)} \rightarrow CO_{2(g)}$$

$$2H_{(ads)} \rightarrow H_{2(g)}$$

On the basis of the adsorption results, we studied the reaction mechanism as shown above for the WGS reaction on the Au_{38} nanoparticle. To perform these mechanistic calculations, we constructed the potential energy surface (PES) by mapping the PES with the NEB method, which is depicted in Figure 6. The important geometric illustrations of intermediates, transition states, and products of the WGS reaction are presented in Figure 7.

In the beginning, CO and H_2O are first coadsorbed to form **IM1** on the Au_{38} nanoparticle. The coadsorption energy is calculated to be −23.55 kcal/mol, which is slightly larger than the sum of the adsorption energies of $CO_{(ads)}$ and $H_2O_{(ads)}$ (−26.58 kcal/mol). In **IM1**, the distance between O atom of H_2O and Au is 2.652 Å which is 0.093 Å longer than that of the H_2O adsorption. This decrease in the binding energy for the coadsorption of CO and H_2O is due in part to the weaker interaction between the H_2O and Au_{38} nanoparticle in the **IM1**. The Bader charge analysis also shows that no charge transfer from the nanoparticle to H_2O occurs (see Table 5).

The dissociation of H_2O from **IM1** into adsorbed OH and H producing **IM2** requires a barrier of 31.41 kcal/mol (**TS1**) with

dx.doi.org/10.1021/jp209172w |*J. Phys. Chem. C* 2012, 116, 336–342

an endothermicity of 20.85 kcal/mol. The broken bond of H−O in **TS1** is 1.351 Å which is ∼0.35 Å longer than that of the H_2O adsorption in the **IM1**. Then the reaction of $OH_{(ads)}$ and $CO_{(ads)}$ produces an $OCOH_{(ads)}$ species by passing **TS2** with a low energy barrier of 1.15 kcal/mol and an exothermicity of 17.14 kcl/mol. In **TS2**, the broken HO−Au bond and forming C−O bond are 2.532 and 1.894 Å, respectively.

The final decomposition of $OCOH_{(ads)}$ occurs by the cleavage of the OCO−H bond and produces $CO_{2(ads)}$ and $H_{(ads)}$. This process requires a barrier of 27.03 kcal/mol. The broken H−O bond of **TS3** is calculated to be 1.371 Å. The adsorption energy of CO_2 is −0.92 kcal/mol, suggesting that the CO_2 molecule is only physisorbed on the Au_{38} nanoparticle. The desorption energy of $2H_{(ads)}$ is only about 2.76 kcal/mol, implying that $H_{2(g)}$ can easily desorb from the Au_{38} nanoparticle surface at room temperature.

In the rate-limiting step ($H_2O_{(ads)} \rightarrow H_{(ads)} + OH_{(ads)}$), the Au_{38} nanoparticle is more reactive because of the lower barrier compared with 35.28 kcal/mol for the Au (100) surface and 32.05 kcal/mol for Au_{29}.[5,6] Our calculations show that the Au_{38} nanoparticle exhibits an activity similar to that of the Cu (111) surface, but lower than the Cu (100) surface and the Cu_{29} nanoparticle for the above rate-limiting step.[5] The reaction barriers of $H_2O_{(ads)} \rightarrow H_{(ads)} + OH_{(ads)}$ on the Cu (111) surface, the Cu (100) surface, and the Cu_{29} nanoparticle are 31.36, 26.06, and 21.44 kcal/mol, respectively;[5,6,46] however, the reaction barrier for $CO_{(ads)} + OH_{(ads)} \rightarrow OCOH_{(ads)}$ on the Au_{38} nanoparticle is much lower than those of the Cu (111) surface, Cu (100) surface, and Cu_{29} nanoparticle (1.15, 8.07, 7.61, and 13.84 kcal/mol for Au_{38}, the Cu (111) surface, the Cu (100) surface, and Cu_{29}, respectively). The desorption of $H_{2(g)}$ also occurs more easily on the Au_{38} nanoparticle than on all the other counterparts, as mentioned above. Accordingly, we predict that the bimetallic Cu−Au catalyst might have the best activity for the WGS reaction because it combines the advantages of the catalytic behavior of Cu and Au metals.

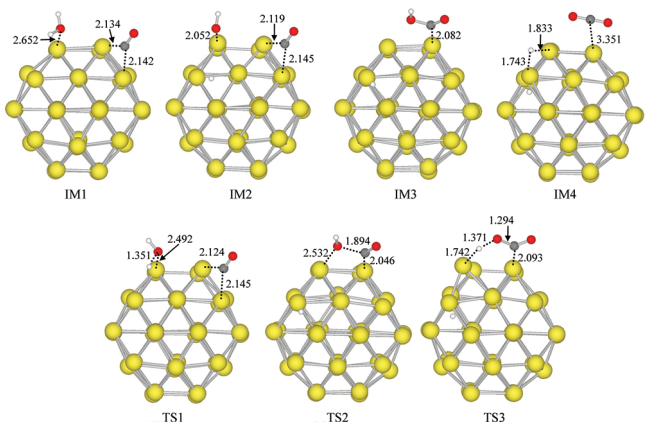

Figure 7. Geometrical illustration of intermediates, transition states, and products for the WGS reaction using the PW91 level of theory. The bond lengths are given in angstroms.

Analysis of the Electronic State During WGS reaction. The electronic local density of states (LDOS) of the system projected on the orbitals for the adsorbed constructs of H_2O (left panel) and CO (right panel) species, as well as the d projected electron density of the bound Au atoms, are depicted in Figure 8. Figure 8a shows the LDOS of the isolated H_2O, CO, and Au_{38} nanoparticle; Figure 8b−h corresponds to the LDOS of **IM1**, **TS1**, **IM2**, **TS2**, **IM3**, **TS3**, and **IM4** configurations, respectively. For the H_2O species on the Au_{38} nanoparticle (see Figures 8b1), there is an overlap between the $3a_1$ and $1b_2$ orbitals of H_2O and the Au d state in **IM1**. As the reaction proceeds, it can be seen that, from **IM1** to **TS1**, orbitals clearly show stronger hybridization (the $3a_1$ and $1b_2$ states vanish abruptly and become broad in a range −3.0 to −6.0 eV) between the H_2O ($3a_1$ and $1b_2$ states) atom and the Au atom (d orbital). As shown in Figure 8d1 (**IM2**), the $1b_1$ state is elevated to interact with the Au d orbital, and a pronounced broadening of the $1b_1$ state occurs at the dissociation of an adsorbed H_2O species. The negatively charged $OH_{(ads)}$ and $H_{(ads)}$ (−0.47 and −0.09*e* for $OH_{(ads)}$ and $H_{(ads)}$) appear from a partial charge transfer from the Au atom, as shown in Table 5.

In Figure 8b2, the shift of the 5σ band of the adsorbed CO to more negative energies results in the overlap between 5σ and 1π states. Pronounced broadening can be found above the Fermi level at **IM1**. It is partially populated due to back-donation of Au d electrons and the charge transfer between the unoccupied orbital $2\pi^*$ of CO with the Au d states, as indicated by the slight increase in the C−O bond length. For **TS1** and **IM2**, the LDOS of the adsorbed CO species remains the same. This is because the $CO_{(ads)}$ does not react with the $H_2O_{(ads)}$. However, the

Table 5. Bader Charge of Au Atoms, C and O1 of CO, and H1, H2, and O2 of H_2O for the Stationary States Along the Minimum Energy Pathway of WGS Reaction on Au_{38} Nanoparticle

	H_2O, CO_2, Au_{38}	Au_{38}−CO	Au_{38}−H_2O	IM1	IM2	IM3	IM4
			CO[a]				
C	0.220	1.707		1.737	1.836	2.489	4.000
O1	−0.220	−1.960		−1.949	−1.968	−1.881	−2.028
			H_2O[a]				
O2	−1.999		−1.978	−1.968	−1.470	−1.891	−2.003
H1	1.000		0.999	1.000	−0.089	−0.109	−1.262
H2	1.000		0.999	1.000	1.000	0.994	−1.236
			Au_{38}[b]				
$Au_{(C1)}$	−0.010	0.082		0.068	0.059	0.139	−0.056
$Au_{(C2)}$	−0.006	0.072		0.068	0.030	−0.008	−0.033
$Au_{(O2)}$	−0.025		0.0455	0.030	0.257	0.025	0.030

[a] O1 represents the O atom of CO; O2 represents the O atom of H_2O. [b] $Au_{(C1)}$, $Au_{(C2)}$, and $Au_{(O2)}$ represent the Au atom bonding with the C atom of CO and the O atom of O2, respectively.

dx.doi.org/10.1021/jp209172w |*J. Phys. Chem. C* 2012, 116, 336–342

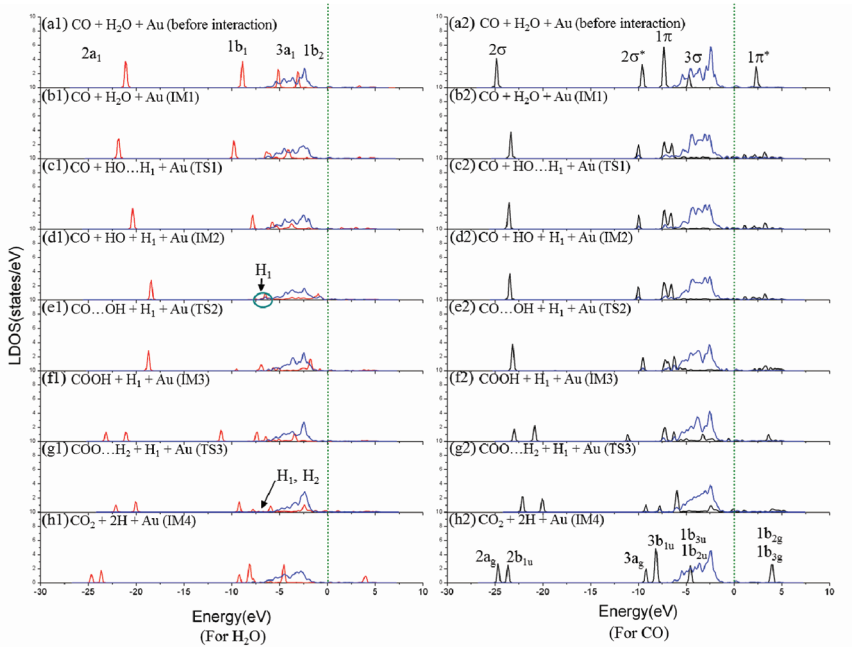

Figure 8. The calculated electronic local density of states of the system projected on the orbitals for the adsorbed constructs of H_2O (left panel) and CO (right panel) species, as well as the d projected of the bound Au atoms. The red, black, and blue lines represent the LDOS of H_2O, CO, and Au(d band), respectively. The dashed line represents the Fermi level.

substantial interaction between the d band of the Au cluster and the nonbonding 5σ state of CO results in a charge transfer from the CO species to $Au_{(C2)}$ in **IM1**, **IM2**, **IM3**, and **IM4** (see Table 5; the $Au_{(C2)}$ becomes more negative) species.

As the reaction proceeds (from Figure 8d to h), the 1b1, 3a1, and 1b2 states of the H_2O species and antibonding orbitals $2\pi^*$ of CO species on the Au nanoparticle spread back and overlap with the Au d state (below the Fermi level). The formation of OCOH adsorbate results in a redistribution of the LDOS, and orbitals shift for both H_2O and CO species. Due to the formation of C−O bond and scission of O−H bond, further interaction between H_2O and CO species is observed distinctly, as shown in Figure 8d−8g. Finally, in Figure 8h, the LDOS for the reaction products is similar to the LDOS of the separated CO_2 gas phase and H adsorbates on the Au_{38} nanoparticle, indicating that the CO_2 molecule is only physisorbed on the nanoparticle.

CONCLUSION

The reaction mechanism of the water−gas shift reaction catalyzed by the Au_{38} nanoparticle as well as adsorption configurations and their electronic properties have been studied at the DFT level in conjunction with the PAW approach. Our results show that the adsorptions OC-B_1 and OC-T_2, H_2O-T_1, HO-B_2, and H-T_1 and H-T_2 are energetically favored among all calculated configurations of H_2O/Au_{38}, CO/Au_{38}, HO/Au_{38}, and H/Au_{38}. A potential energy surface for the WGS reaction on the Au_{38} nanoparticle has been constructed using the NEB method. Compared with the Au (100) surface and Au_{29}, the Au_{38} nanoparticle is more reactive as a result of the lower barrier of the rate-limiting step ($H_2O_{(ads)} \rightarrow H_{(ads)} + OH_{(ads)}$). Compared with Cu-related materials, the Au_{38} nanoparticle exhibits activity similar to the Cu (111) surface but lower than the Cu (100) surface and Cu_{29} nanoparticle in terms of reaction barrier of the rate-limiting step. However the reaction barrier for $CO_{(ads)} + OH_{(ads)} \rightarrow OCOH_{(ads)}$ is much lower than those of the Cu (111) surface, Cu (100) surface, and Cu_{29} nanoparticle. The desorption of $H_{2(g)}$ also occurs more easily on the Au_{38} nanoparticle than the other counterparts, as mentioned previously. Accordingly, we predict that the bimetallic Cu−Au catalyst has better activity for WGS reaction than the single component nanoparticle, such as Au and Cu, as it combines the advantages of the catalytic behavior of Cu and Au metals.

AUTHOR INFORMATION

Corresponding Author

*E-mails: (F.-Y.L.) feng64@dragon.nchu.edu.tw, (H.-T.C.) htchen@cycu.edu.tw.

ACKNOWLEDGMENT

We are grateful to (1) the National Science Council, Republic of China, under Grant No. NSC 99-2113-M-033-009-MY2 for financial support and (2) the National Center for High-performance Computing, Taiwan, for computer time and facilities.

REFERENCES

(1) Liu, Y.; Fu, Q.; Flytzani-Stephanopoulos, M. *Catal. Today* **2004**, *93−95*, 241.
(2) Song, C. *Catal. Taday* **2002**, *77*, 17.
(3) Suh, D. J.; Kwak, C.; Kim, J. H.; Kwon, S. M.; Park, T. J. *J. Power Sources* **2005**, *142*, 70.
(4) Ruettinger, W.; Ilinich, O.; Farrauto, R. J. *J. Power Sources* **2003**, *118*, 61.
(5) Rodriguez, J. A. ; Liu, P.; Hrbek, J.; Evans, J.; Perez, M. *Angew. Chem., Int. Ed.* **2007**, *46*, 1329.
(6) Liu, P.; Rodriguez, J. A. *J. Chem. Phys.* **2007**, *126*, 164705.
(7) Koryabkina, N. A.; Phatak, A. A.; Ruettinger, W. F.; Farruto, R. J.; Rebeiro, F. H. *J. Catal.* **2003**, *217*, 233.

(8) Geissler, K.; Newson, E.; Vogel, F.; Truong, T.-B.; Hottinger, P.; Wokaun, A. *Phys. Chem. Chem. Phys.* **2001**, *3*, 289.
(9) Cortright, R. D.; Davda, R. R.; Dumesic, J. A. *Nature* **2002**, *418*, 964.
(10) Choi, Y.; Stenger, H. G. *Appl. Catal., B* **2002**, *38*, 259.
(11) Haruta, M. *Catal. Today* **1997**, *36*, 153–166.
(12) Haruta, M. *Nature* **2005**, *437*, 1098–1099.
(13) Haruta, M.; Kobayashi, T.; Sano, H.; Yamada, N. *Chem. Lett. (Jpn)* **1987**, *16*, 405–408.
(14) Turner, M.; Golovko, V. B.; Vaughan, O. P. H; Abdulkin, P.; Berenguer-Murcia, A.; Tikhov, M. S.; Johnson, B. F. G.; Lambert, R. M. *Nature* **2008**, *454*, 981–983.
(15) Valden, M.; Lai, X.; Goodman, D. W. *Science* **1998**, *281*, 1647–1650.
(16) Haruta, M.; Tsubota, S.; Kobayashi, T.; Kageyama, H.; Genet, M. J.; Delmon, B. *J. Catalys.* **1993**, *144*, 175–192.
(17) Carrettin, S.; Concepción, P.; Corma, A.; Nieto, J. M. L.; Puntes, V. F. A. *Chem., Int. Ed.* **2004**, *43*, 2538.
(18) Gluhoi, A. C.; Dekkers, M. A. P.; Nieuwenhuys, B. E. *J. Catal.* **2003**, *219*, 197.
(19) Grisel, R. J. H.; Nieuwenhuys, B. E. *J. Catal.* **2001**, *199*, 48.
(20) Romero-Sarria, F.; Martinez, L. M.; Centeno, M. A.; Odriozola, J. A. *J. Phys. Chem. C* **2007**, *111*, 14469.
(21) Sanchez, A.; Abbet, S.; Heiz, U.; Schneider, W.-D.; Häkkinen, H.; Barnett, R. W.; Landman, U. *J. Phys. Chem. A* **1999**, *103*, 9573.
(22) Schubert, M. M.; Hackenberg, S.; Van Veen, A. C.; Muhler, M.; Plzak, V.; Behm, R. J. *J. Catal.* **2001**, *197*, 113.
(23) Chang, C. M.; Cheng, C.; Wei, C. M. *J. Chem. Phys.* **2008**, *128*, 124710.
(24) Gao, W.; Chen, X. F.; Li, J. C.; Jiang, Q. *J. Phys. Chem. C* **2010**, *114*, 1148.
(25) Garzón, I. L.; Michaelian, K.; Beltrán, M. R.; Posada-Amarillas, A.; Ordejón, P.; Artacho, E. *Phys. Rev. Lett.* **1998**, *81*, 1600.
(26) Liu, P.; Rodriguez, J. A. *J. Chem. Phys.* **2007**, *126*, 164705.
(27) Lopez, N.; Nørskov, J. K. *J. Am. Chem. Soc.* **2002**, *124*, 11262–11263.
(28) Remediakis, I. N.; Lopez, N.; Nørskov, J. K. *Angew. Chem., Int. Ed.* **2005**, *44*, 1824.
(29) Wang, Y.; Gong, X. G. *J. Chem. Phys.* **2006**, *125*, 124703.
(30) Chen, H.-T.; Chang, J.-G.; Ju, S.-P.; Chen, H.-L. *J. Comput. Chem.* **2010**, *31*, 258. Chen, H.-T.; Chang, J.-G.; Ju, S.-P.; Chen, H.-L. *J. Phys. Chem. Lett* **2010**, *1*, 739.
(31) Hohenberg, P.; Kohn, W. *Phys. Rev. B* **1964**, *136*, 864.
(32) Kresse, G.; Furthmuller, J. *Comput. Mater. Sci.* **1996**, *6*, 15.
(33) Kresse, G.; Hafner, J. *Phys. Rev. B* **1993**, *47*, 558.
(34) Kresse, G.; Hafner, J. *Phys. Rev. B* **1994**, *49*, 14251.
(35) Kresse, G.; Hafner, J. *J. Phys.: Condens. Matter* **1994**, *6*, 8245.
(36) Kresse, G.; Hafner, J. *Phys. Rev. B* **1996**, *54*, 11169.
(37) Perdew, J. P.; Burke, K.; Ernzerhof, M. *Phys. Rev. Lett.* **1996**, *77*, 3865.
(38) Perdrw, J. P.; Yang, Y. *Phys. Rev. B* **1992**, *45*, 244.
(39) Henkelman, G.; Uberuaga, B. P.; Jónsson, H. *J. Chem. Phys.* **2000**, *113*, 9901.
(40) Mills, G.; Jónsson, H.; Schenter, G. K. *Surf. Sci.* **1995**, *324*, 305.
(41) Bader, R. F. W. *Atoms in Molecules - A Quantum Theory*; Clarendon Press: Oxford, 1994.
(42) Bader, R. F. W.; Beddall, P. M. *J. Chem. Phys.* **1972**, *56*, 3320.
(43) Henkelman, G.; Arnaldsson, A.; Jónsson, H. *Comput. Mater. Sci.* **2006**, *36*, 354.
(44) Häberlen, O. D.; Chung, S.-C.; Stener, M.; Rösch, N. *J. Chem. Phys.* **1997**, *106*, 5189.
(45) Delbecq, F.; Zaera, F. *J. Am. Chem. Soc.* **2008**, *130*, 14924.
(46) Gokhale, A. A.; Dumesic, J. A.; Mavrikakis, M. *J. Am. Chem. Soc.* **2008**, *130*, 1402–1414.